

Article

Thiol–Ene Photopolymerization: Scaling Law and Analytical Formulas for Conversion Based on Kinetic Rate and Thiol–Ene Molar Ratio

Kuo-Ti Chen ¹, Da-Chuan Cheng ², Jui-Teng Lin ³ and Hsia-Wei Liu ^{4,*}

¹ Graduate Institute of Applied Science and Engineering, Fu Jen Catholic University, New Taipei City 24205, Taiwan; tony022199@msn.com

² Department of Biomedical Imaging and Radiological Science, China Medical University, Taizhong 400, Taiwan; dccheng@mail.cmu.edu.tw

³ New Vision, Inc., New Taipei City 242, Taiwan; jtlin55@gmail.com

⁴ Department of Life Science, Fu Jen Catholic University, New Taipei City 24205, Taiwan

* Correspondence: 079336@gmail.com; Tel.: +886-0910-688-968

Received: 22 September 2019; Accepted: 7 October 2019; Published: 10 October 2019



Abstract: Kinetics and analytical formulas for radical-mediated thiol–ene photopolymerization were developed in this paper. The conversion efficacy of thiol–ene systems was studied for various propagation to chain transfer kinetic rate-ratio (R_K), and thiol–ene concentration molar-ratio (R_C). Numerical data were analyzed using analytical formulas and compared with the experimental data. We demonstrated that our model for a thiol–acrylate system with homopolymerization effects, and for a thiol–norbornene system with viscosity effects, fit much better with the measured data than a previous model excluding these effects. The general features for the roles of R_K and R_C on the conversion efficacy of thiol (C_T) and ene (C_V) are: (i) for $R_K = 1$, C_V and C_T have the same temporal profiles, but have a reversed dependence on R_C ; (ii) for $R_K \gg 1$, C_T are almost independent of R_C ; (iii) for $R_K \ll 1$, C_V and C_T have the same profiles and both are decreasing functions of the homopolymerization effects defined by k_{CV} ; (iv) viscosity does not affect the efficacy in the case of $R_K \gg 1$, but reduces the efficacy of C_V for other values of R_K . For a fixed light dose, higher light intensity has a higher transient efficacy but a lower steady-state conversion, resulting from a bimolecular termination. In contrast, in type II unimolecular termination, the conversion is mainly governed by the light dose rather than its intensity. For optically thick polymers, the light intensity increases with time due to photoinitiator depletion, and thus the assumption of constant photoinitiator concentration (as in most previous models) suffers an error of 5% to 20% (underestimated) of the crosslink depth and the efficacy. Scaling law for the overall reaction order, defined by $[A]^m[B]^n$ and governed by the types of ene and the rate ratio is discussed herein. The dual ratio (R_K and R_C) for various binary functional groups (thiol–vinyl, thiol–acrylate, and thiol–norbornene) may be tailored to minimize side effects for maximal monomer conversion or tunable degree of crosslinking.

Keywords: thiol–ene functional group; kinetic model; photopolymerization; crosslinking; curing depth

1. Introduction

Photopolymerization and crosslinking have been utilized in various medical and industrial applications [1–5]. Compared to thermal-initiated polymerization, photo-initiated polymerization provides the advantages of fast and controllable reaction rates and spatial and temporal control over the formation of the material without the need for high temperatures or harsh conditions [1,2]. Tissue engineering using scaffold-based procedures for chemical modification of polymers has been reported

to improve their mechanical properties by crosslinking or polymerization with UV or visible light to produce gels or high-molecular-weight polymers [3]. Industrial applications to date include the development of materials for thin films, 3D bio-printing, and microfabrication [5–7], in which the kinetics and mechanisms of photopolymerization have been extensively studied theoretically and experimentally [7–18].

The UV curing system is roughly categorized into three units: the radical system, cationic system, and anionic system. The radical system is mainly used for conventional UV curing systems. Thiol–ene photopolymerization (TEP) is based on the radical catalyzed addition of a thiol to a vinyl functional group, in which cross-linked polymer networks are formed via a two-step growth mechanism: (i) propagation of a thiyl radical through a vinyl functional group, (ii) followed by chain transfer from the resulting carbon radical to a thiol functional group, regenerating the thiyl radical [18–22]. In comparison, thiol–Michael photopolymerization (TMP) involves anion-mediated addition of a multifunctional thiol to an electron-deficient vinyl group of a multivinyl component [23–27]. Both TEP and TMP exhibit the advantages of typical photopolymerizations, including rapid reaction, optical clarity, negligible oxygen inhibition, solvent tolerance, high reaction yields, excellent mechanical properties, and they do not require solvents for processing [21–23]. In addition, TMP exhibits delayed gelation, and minimal byproduct formation and homopropagation effect of the vinyl group. Depending on the specific ene selected, TEP generally proceeds via a step-mode or mixed-mode chain-growth radical mechanism, and exhibits reaction kinetics strongly dependent on the electronic density of the ene (electron-rich vs. electron-poor) as well as the thiol and ene structures [18,19]. Both computational and experimental investigations have been performed to evaluate the role of solvents, monomers, and catalysts on this reaction mechanism [18–27].

The mechanism and kinetics of TEP utilizing a tetrafunctional thiol monomer copolymerized with acrylate, norbornene, vinyl ether, and vinyl-silazane-functionalized ene monomers were modeled and experimentally characterized by Cramers et al. [18] and Reddy et al. [20]. They demonstrated that reaction orders in TEP systems are controlled by the ratio of thiyl radical propagation (k_p) to chain transfer (k_{CT}) kinetic parameters, $R_K = k_p/k_{CT}$, which is also related to the electron density of the vinyl group and the carbon radical stability, which could provide spatiotemporal control over the course of the reaction. The scaling law for the functional group concentration of thiol, [A], and ene, [B], given by $[A]^m[B]^n$, with m and n ranging from 0 to 2, is related to the type of ene and the rate ratio. For example, for $R_K \gg 1$, polymerization rates are first order in ene concentration (or $n = 1.0$) and nearly independent of the thiol concentration (or $m = 0$); in contrast, $m = 1.0$ and $n = 0$ for $R_K \ll 1$. For R_K values near unity, polymerization rates are approximately 0.5 order in both the thiol and ene functional group concentrations ($m = n = 0.5$). However, a scaling law of $m = 0.4$ and $n = 0.6$ has been found in an acrylate system (with $R_K = 13$) due to contributions from homopolymerization [18].

In general, competitive propagation/chain transfer process must occur, with one of the elementary reaction steps often becoming rate-limiting. These processes also determine the rate-limiting step and time to reach the gel-point conversion [24]. The temporal profiles of thiol and ene functional groups were successfully modeled and compared with measured data by Cramers et al. [18] with various rate-ratio R_K and concentration-ratio R_C , except for the thiol–norbornene system which has a strong viscosity effect. Therefore, their model excluding the viscosity effect predicted a higher efficacy than their measured data. Although Cramers et al. [18] presented the temporal profiles of the functional groups based on numerical solutions, however, no analytical formulas were reported. Most of the previous models [18–27] have been based on oversimplified assumptions of constant photoinitiator (PI) or photosensitizer (PS) concentration (without depletion), and thus the light intensity in these models follows the conventional Beer–Lambert law (BLL), which is only valid for optically thin polymers and will suffer huge errors in optically thick polymers [15,16].

This study will focus, for the first time, on the analytical formulas for the conversion efficacy for various kinetic rate ratios and functional group concentration molar ratios. A set of more general kinetic rate equations was derived, including viscosity and homopolymerization effects. Numerical data were

analyzed using our analytic formulas and compared with the experimental data of Cramers et al. [18]. We also demonstrated that our model for a thiol–acrylate system including homopolymerization effects, and for a thiol–norbornene system including viscosity effects, fit much better with the measured data than the model of Cramers et al. [18]. Furthermore, the dynamic light intensity resulted by the PI depletion has been discussed, in which the optically thin assumption in previous models [18–27] caused errors of 5% to 20% on crosslink depth and efficacy. We have also discussed the scaling law for the overall reaction order, defined by $[A]^m[B]^n$, and governed by the types of ene and the rate ratios. This study provides useful guidance for free radical photopolymerization via the roles of the dual ratios (R_K and R_C) in various binary functional groups, including thiol–vinyl, thiol–acrylate, and thiol–norbornene.

2. Materials and Methods

2.1. Photochemical Kinetics

As shown in Figure 1, a two-monomer system [A] and [B] involves three crosslinking pathways: two radical-mediated (or electron transfer) pathways (1 and 2), and one oxygen-mediated (or energy transfer) pathway (3). The ground state photosensitizer (PS) is excited to its triplet excited state T^* by a quantum yield (q). In a type I process, T^* interacts directly with [A] and [B] to form the intermediate radicals R' and S' , which then produce the reactive R and S which could interact with oxygen 3O_2 , [A], [B], or bimolecular terminations R^2 and S^2 . For a type II (or oxygen-mediated) process, T^* interacts with 3O_2 to form a singlet oxygen 1O_2 , which could interact with [A], [B], or be relaxed to 3O_2 . Both type I and type II reactions can occur simultaneously in photopolymerization, and the ratio between these processes depends on the type of photosensitizer (PS) or photoinitiator (PI) used, the concentrations of PS or PI, substrate monomers and oxygen, the kinetic rates involved in the process, and the light intensity, dose, PI depletion rate, etc. Greater details of these kinetics were published in our earlier work [13–15]. In a thiol–ene polymerization system, the functional groups are insensitive to oxygen inhibition; therefore, it can be treated as a type-I-dominant system.

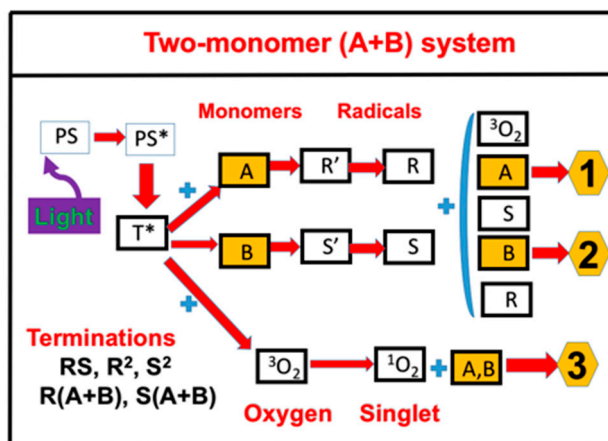


Figure 1. Schematics of three photochemical pathways in a two-monomer system, A and B, in the presence of ground state oxygen 3O_2 , for radical-mediated pathways (1 and 2), and oxygen-mediated pathway (3). PS is the ground state photosensitizer (PS), having excited and triplet states PS^* and T^* ; terminations include unimolecular, bimolecular recombination, and inter-radical coupling [15,17].

For a thiol–ene system, as shown in Figure 2, the photochemical pathways are more simple and can be shown by two-step growth mechanism, which involves (i) propagation of a thiol radical (R) through an ene functional group [B] to form a carbon radical (S), and (ii) chain transfer from the resulting carbon radical (S) to a thiol functional group [A], regenerating the thiol radical (R) which

reacts with [A] to form the reaction cycle, where R and S could be coupled and also terminated by bimolecular recombination, or react with [A] and [B] in general.

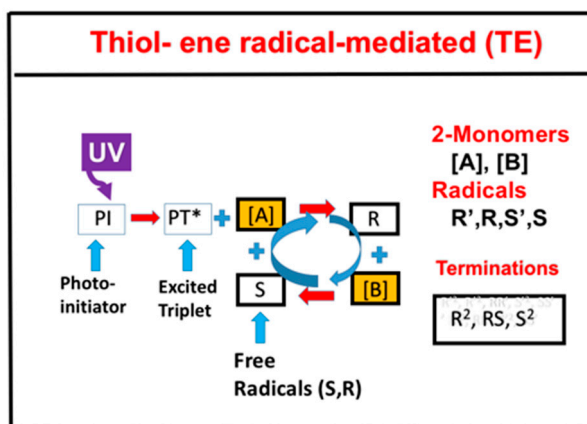


Figure 2. Schematics of UV-light initiated photopolymerization kinetics of thiol [A] and ene [B] functional groups, in which the thiol radical R reacts with [B] to form a carbon radical (S), which reacts with the thiol and regenerates R to form the reaction cycle; R and S could interact with each other or be terminated by bimolecular recombinations, S² and R².

The thiol–ene pathways of Figure 2 are a special situation of the more general pathways of Figure 1, where the functional groups are insensitive to oxygen inhibition and can be treated as a type-I-dominant system, neglecting oxygen-mediated type II reactions. In addition, thiol monomer, [B], do not couple directly with thiol radical (R), but with the carbon radical (S) to regenerate R to form the reaction cycle. Therefore, the rate equations for thiol–ene system (Figure 2) are the reduced form of the two-monomer system (Figure 1). For simplicity, the intermediate radicals in Figure 2 (R' and S') are not shown in the kinetic scheme, but they have been included in our kinetic equations and calculations.

Using the following short-hand notation: C for the concentration of PI ground state (with an initial value C₀); [A] and [B] for the concentrations of the thiol and ene functional groups; [R'] and [S'] for the intermediate radicals, and [R] and [S] for the reactive radicals, we obtained a set of general rate equations associated with the two-monomer system shown by Figure 2, as follows [13,17].

$$\frac{\partial C}{\partial t} = -bI_g([A] + [B] + k_g' C [O_2])C + R_E \tag{1}$$

$$\frac{dI(z, t)}{dz} = -A(z, t)I(z, t) \tag{2}$$

$$\frac{\partial [R]}{\partial t} = 2k_{T1}[R']^2 - (2k_{T1}[R]^2 + k_{12}[R][S] + k''[R][O_2]) - G \tag{3}$$

$$\frac{\partial [S]}{\partial t} = 2k_{T2}[S']^2 - (2k_{T2}[S]^2 + k_{12}[R][S] + k''[S][O_2]) + G \tag{4}$$

$$\frac{\partial [O_2]}{\partial t} = -[bI_g C + k''([R] + [S])][O_2] + P \tag{5}$$

$$\frac{\partial [A]}{\partial t} = -R_T [A] \tag{6}$$

$$\frac{\partial [B]}{\partial t} = -R_T [B] \tag{7}$$

$$R_T = bI_g C + k''([R] + [S]) \tag{8}$$

$$G = k_{41}[R][A] - k_{42}[S][B] \tag{9}$$

$$A(z, t) = 2.3[(a' - b')C + b'C_0 + Q] \quad (10)$$

where $b = aqI(z,t)$; q is the quantum yield of the PI excited state; $a = 83.6wa'$; w is the wavelength of light (in cm); and $I(z,t)$ is the light intensity with a unit of mW/cm^2 . a' and b' are the molar extinction coefficients (in $1/mM/\%$) of the initiator and the photolysis product, respectively; and Q is the absorption coefficient of the monomer and the polymer repeat unit.

R_E is the regeneration of PI ground state given by $R_E = (k_{91}[R] + k_{92}[S])[O_2] + 2k_{T1}R^2 + 2k_{T2}S^2$; $g = 1/(k_{57} + k_{37}[O_2] + [A] + [B])$, $g' = 1/(k_{68} + k_{48}C + [A] + [B])$, $k = (k_{11}/k_8)$; $k_{37} = k_3/k_7$, $k_{57} = k_5/k_7$; $k_{68} = k_6/k_8$, $k_{48} = k_4/k_8$, where k_5 and k_3 are the relaxation rate of the PI triplet state (T^*) and the coupling rate of T^* and oxygen; k_{71} and k_{72} are the coupling rate of T^* and monomers [A] and [B]; k_{88} , k_{81} , and k_{82} are the coupling rates of singlet oxygen and monomers; k_{41} , k_{42} , k_{51} , and k_{52} are the coupling of radicals R and S and monomers. Greater detail and derivation of the above equations may be found in References [13,15], which also show the kinetic equations for the triplet state (T^*) and singlet oxygen [X]. Therefore, Equation (1) to (10) of this article describe the quasi-steady-state form of Equation (1) from Reference [13] under the quasi-steady-state condition $dT^*/dt = d[X]/dt = 0 = d[R']/dt = d[S']/dt = 0$, which also defines the steady-state value of radicals [R'] and [S']. Substituting these values into Equations (3) and (4), we obtain the steady-state reactive radicals [R] and [S]:

$$2k_{T1}[R]^2 + k[R][O_2] + G - bICg[A] = 0 \quad (11)$$

$$2k_{T2}[S]^2 + k'[S][O_2] - G - bICg[B] = 0 \quad (12)$$

For a thiol-ene system, which has the advantages of being relatively uninhibited by oxygen. Therefore, we may ignore the oxygen related terms $k''[R][O_2]$ and $k''[S][O_2]$, in Equations (1) to (10). Without oxygen inhibition, $k_{57} \ll [A] + [B]$, $g([A] + [B]) = 1$ for $k_{72} = k_{71}$, and $g'[O_2] = 0$. We further assumed, as proposed by Cramer et al. [10], that the consumption rates of the thiol and ene functional groups could be set as equal, $d[A]/dt = d[B]/dt$, which allowed us to solve for Equations (6) and (7) for [S], thus solving Equation (11) for [R]. Substituting these steady-state values, [S] and [R], into Equation (8), we obtained the simplified rate equations of monomers [A] and [B] as follows.

$$\frac{d[A]}{dt} = -R_p \quad (13)$$

$$\frac{d[B]}{dt} = -R_p(1 + H_M) \quad (14)$$

$$R_p = K \sqrt{0.5bIC/G} \quad (15)$$

$$G = (Fk_p[B])^{-2} + (k_{CT}[A])^{-2} + (Fk_p k_{CT}[B][A])^{-1} \quad (16)$$

$$H_M = (k_{CV}/k_{CT})([B]/(D[A])) \quad (17)$$

where H_M is the revised term for the homopolymerization effect, with $D = 1 + k_{CT}[B]/(Fk_p[A])$. $K = k_p/k_T^{0.5}$ is an effective rate constant; $k_{52} = k_{CT}$, $k_{T1} = k_{T2} = k_T$, are, respectively, the rate constants for chain transfer, propagation, and termination; and $k_{52} = k_{CV}$ is the rate of the homopolymerization effect, H_M , which is given by the $k_{52}[B]$ term of Equation (9); however, we ignored the $k_{51}[A]$ term, since [A] (thiol) has weaker homopolymerization than [B] (ene).

In Equation (16), we also revised the propagation rate constant k_p , by a reduction factor (F) for the viscosity effect on the ene, given by $F = 1 - d'C_{EFF}$, where d' is a fit reduction rate and C_{EFF} is the conversion efficacy of the ene group given by $C_{EFF} = 1 - \exp(-S)$, where S is given by the time integral of $[A]/[A]_0$, or the solution of Equation (13). The viscosity effect reduces the available free volume or decreases k_p in the diffusion-controlled region [11]. Without the extra two consumption terms of the ene group viscosity and homopolymerization effects, $H_M = 0$ (or $k_{CV} = 0$) and $F = 1$, Equations (13) and (14) have the same total reaction rate function, R_p , which is symmetric with regards to [A]

and [B] such that their conversion efficacies are also symmetrically related. These features are further demonstrated later in the paper by our numerical data.

The above revised kinetic equations can be reduced to those of Cramer et al. [18] under the following three assumptions: (i) homopolymerization and viscosity effects are neglected (with $H_M = 0$ and $F = 1$); (ii) the PI concentration is a constant, or Equation (1) $dC/dt = 0$ (or $bIt \ll 1$, for small doses), and (iii) light intensity is a constant, or Equation (2), $dI/dt = dI/dz = 0$, which is valid only for a short exposure time, or an optically thin polymer.

Accurate solutions of Equations (13) to (17) require numerical simulations. For analytical formulas, we used approximated analytic formulas for the light intensity and the PI concentration, such that we did not need to solve for Equation (1), and the expressive closed forms of $I(z,t)$ and $C(z,t)$ allowed us to solve analytically for the first-order solutions of Equations (13) and (14) for the chain and propagation limited cases.

2.2. Analytical Formulas for Efficacy

The monomer conversion efficacy for a bimolecular termination process is given by $C_{EFF} = 1 - [M]/[M]_0 = 1 - \exp(-S)$ with $[M] = [A]$ or $[B]$, and the S function is given by the solution of Equations (13) and (14) as follows. Analytical solutions are available for the two limiting cases defined by the ratio of chain (k_p) and propagation rate (k_{CT}), defined as $R_K = k_p / k_{CT}$: in Case i, $k_p \ll k_{CT}$ (chain limited), and in Case ii, $k_p \gg k_{CT}$ (propagation limited).

For Case i, $k_p[B] \ll k_{TC}[A]$, Equation (15) becomes

$$R_p = K \sqrt{0.5bIC} Fk_p[B] \tag{18}$$

Using the above R_p and solving for the first-order solution of Equation (14), for the case of $F = 1$ (viscosity effect is neglected) and $F' = 0$ (or homopolymerization effect is neglected), we obtained the first-order solution of $[A]$ and $[B]$, which allowed us to calculate F' and the conversion efficacy of the ene, $C_V = 1 - [B]/[B]_0$,

$$C_V = 1 - \exp(-S) \tag{19}$$

$$S = \int_0^t K F k_p (1 + H_M) \sqrt{0.5bIC} dt \tag{20}$$

which also gives $[B] = [B]_0 \exp(-S)$, and solve for Equation (13); thus, we obtained the conversion efficacy of the thiol, defined by $C_T = 1 - [A]/[A]_0$,

$$C_T = 1 - ([B]_0/[A]_0) S_T \tag{21}$$

$$S_T = \int_0^t K F k_p \sqrt{0.5bIC} \exp(-S) dt \tag{22}$$

For Case ii, $k_p[B] \gg k_{TC}[A]$, Equation (15) becomes

$$R_p = K \sqrt{0.5bIC} k_{CT}[A] \tag{23}$$

Similarly, solving for Equations (13) and (14), we obtained the second-order conversion efficacy for thiol (C_T) and ene (C_V), as follows.

$$C_T = 1 - \exp(-S') \tag{24}$$

$$S' = \int_0^t K k_{CT} \sqrt{0.5bIC} dt \tag{25}$$

$$C_V = 1 - ([A]_0/[B]_0)S_V \tag{26}$$

$$S_V = \int_0^t Kk_{CT}(1 + H_M) \sqrt{0.5bIC} \exp(-S') dt \tag{27}$$

2.3. The Second-Order Solution

Equations (19) to (27) are the first-order solutions for the limiting cases of $k_P[B] \gg k_{TC}[A]$ and $k_P[B] \ll k_{TC}[A]$. To include the high-order terms for the case of comparable k_P and k_{CT} with $k_P[B] > k_{TC}[A]$, Equation (22) was revised to $(1 - d)S$, with $d = (k_P/k_{CT}) [B']/[A']$, which is a decreasing function of the first-order solution product $[B']/[A']$. Therefore, the conversion efficacy of $[B]$ is an increasing function of the concentration ratio $[A]_0/[B]_0$. Similarly, for $k_P[B] < k_{TC}[A]$, Equation (25) was revised to $(k_{CT}/k_P) (1 - 1/d) S'$, which is a decreasing function of $[A']/[B']$. Therefore, the conversion efficacy of $[A]$ is a decreasing function of $[A]_0/[B]_0$. This feature of the conversion efficacy of $[A]$ and $[B]$ can be seen by the symmetrical formulas, as shown by Equations (21) and (26). This feature is consistent with the measured data shown in Figure 3 of Cramer et al. [18] for a thiol–vinyl ether system with $k_P = 1.2k_{CT}$. The common feature is that for $k_P = k_{CT}$, the conversions of $[A]$ and $[B]$ have symmetrical formats and are proportional to the ratios $[A]_0/[B]_0$ and $[B]_0/[A]_0$, respectively. This symmetry is broken when k_P and k_{CT} are not equal, or when there are other consumption factors of $[B]$, such as viscosity or homopolymerization effects. Greater details are discussed later.

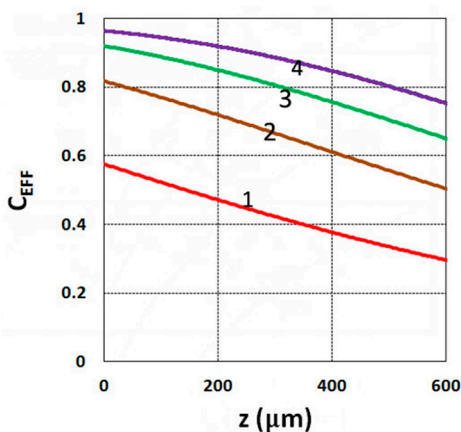


Figure 3. Conversion efficacy vs. depth (z) for $t = (10, 20, 30, 40)$ s, given by curves 1, 2, 3, and 4, respectively, for a fixed light intensity $I_0 = 3 \text{ mW/cm}^2$, $C_0 = 0.1\%$, $b = 0.001$, $a' = 130 \text{ (1/cm/mol)}$, $K = 5.0$, $b' = Q = 0$, $B' = 0$.

2.4. Effects of Viscosity and Homopolymerization

To include the effects of homopolymerization given by H_M , the first-order solutions of $[A]$ and $[B]$ can be substituted into Equation (20) for the H_M function; we thus obtained the second-order conversion efficacy defined by a revised S -function of Equation (20), which resulted a higher efficacy for $[B]$ and $[A]$, as predicted by Equation (20), for the case of $k_P[B] \ll k_{TC}[A]$. In comparison, when $k_P[B] \gg k_{TC}[A]$, H_M does not affect the first-order solution of $[A]$, as shown by Equation (25), but it reduces the efficacy of $[B]$, as shown by Equation (27). We confirmed these features by numerical solution, as detailed later in the paper.

To include the viscosity effects, or when $F < 1$ in Equation (16), the free volume was reduced when crosslink efficacy increased. The reduction factor (F) only affected the propagation rate constant Fk_P in Equation (17), but not that in Equation (23). Therefore, it only reduced the efficacy of $[B]$. We propose $F = 1 - [1 - \exp(-S')]$, with S' proportional to the efficacy and given by a fit function $S' = 2[1 - \exp(-mb'I_0t)]/(mb'I_0)^{0.5}$, where m and b are fit parameters to be found later by comparing

with the measured data. The reduction factor is proportional to the available free volume, or a decreasing function of the conversion efficacy, which is proportional to S' . To include both the homopolymerization and viscosity effects, F and F' are needed to solve for Equation (3). Numerical solutions, shown later, demonstrated the above features predicted by our analytical formulas.

2.5. Dynamic Light Intensity

Solving Equations (1) and (2) for the light intensity, $I(z,t)$, and PI concentration, $C(z,t)$, concentration, we numerically found S and S' and then the conversion functions, C_V and C_T . We further derived the analytical form of conversion efficacy, which required closed forms of $I(z,t)$ and $C(z,t)$, as follows. Using our previously developed approximated analytical formulas [13,15]

$$I(z,t) = I_0 \exp[-A'z] \quad (28)$$

$$C'(z,t) = C_0 \exp[-Bt] \quad (29)$$

$$A'(z,t) = 2.3(a'C_0 + Q) - B't \quad (30)$$

where $B = bI_0 \exp(-A''z)$, $B' = 2.3(a' - b')C_0I_0bz$, with A'' as the averaged absorption given by $A'' = 1.15(a' + b')C_0 + 2.3Q$. Note that the $-B't$ term represents the decrease of A' , or increase of light intensity due to PI depletion. Equation (29) is the approximated solution of Equation (1) with oxygen ignored, or $k_{88}[X] = 0$ and $g[A] + g'[B] = 1$. Using Equations (28) and (29), we obtained the analytical form of Equation (20) for the cases of $F = 1$ and $F' = 0$:

$$S = K \sqrt{0.5bXI_0C_0} E(z,t) \quad (31)$$

$$E(z,t) = [1 - \exp(-B''t)]/B'' \quad (32)$$

where $B'' = 0.5(B - B')$ and $X = \exp[-2.3(a'C_0 + Q)z]$. Equation (31) gives the close form of Equation (20) for C_V , and also allowed us to numerically integrate Equation (6) to obtain C_T for Case i. Similarly, for Case ii and Equation (25), $S' = (k_{CT}/k_P)S$, which gave a close form of C_V , and C_T from Equation (27). Note that Equation (30) defines the dynamic feature of the light intensity, which is an increasing function of time due to the depletion of the PI concentration. It also provides the nonlinear depth (z) dependence of $A'z$, given by B' . The above analytical formulas provide useful information with which to analyze and predict the critical roles of each of the influencing factors without numerically solving the coupled equations.

2.6. Gelation Time

The critical (gelation point) conversion, C_{CT} , may be defined by the classical Flory–Stockmayer equation [10]:

$$C_{CT} = 1/\sqrt{R_C(f_T - 1)(f_V - 1)} \quad (33)$$

where f_T and f_V are the functionalities of thiol and ene monomers, respectively; and $R_C = [A]_0/[B]_0$ is the thiol–ene stoichiometric initial molar ratio. For the case of neglected induction time, we found that the gelation time can be given by solving the exposure time of Equations (31) and (6) under the critical condition of Equation (33). For example, for the case of $k_P[B] \ll k_{TC}[A]$, we solved for Equations (31) and (33) to obtain the gelation time (T_{GEL}) for the ene:

$$T_{GEL} = (1/B'') \ln[1/(1 - B_1)] \quad (34)$$

$$B_1 = B''L/(K\sqrt{0.5b}) \quad (35)$$

$$L = \ln[1/(1 - C_{CT})] \quad (36)$$

Similarly, we obtained the gelation time for the case of $k_P[B] \gg k_{TC}[A]$ given by Equation (20), given by the same formula as Equation (34), but Equation (35) was revised to:

$$B_1 = B''L / [k_{TC}K \sqrt{0.5b}] \tag{37}$$

However, there are no analytic formulas for C_T for the case of $k_P[B] \ll k_{TC}[A]$, or C_V for the case of $k_P[B] \gg k_{TC}[A]$ due to the complex integrations of Equations (20) and (25).

2.7. Crosslink Depth

A crosslink depth (Z_C) is defined by when the conversion efficacy is higher than a critical value, $C_T > C_{CT}$, or when $S > S_{CT}$ with $S_{CT} = \ln [1/(1 - C_{CT})]$. Using Equation (31), and with $S = S_{CT} = 2$ (or $C_{CT} = 0.86$), Z_C is related to the crosslink time (T_C) by:

$$T_C = \left(\frac{1}{B''} \right) \ln \left[2B'' / \left(K \sqrt{0.5bXI_0C_0} \right) - 1 \right] \tag{38}$$

Note that Equation (38) is a nonlinear function of Z_C ; therefore, there is no analytical formula for Z_C vs. T_C . However, this formula can be found by plotting the curve of T_C vs. Z_C , then rotating the axis to show the curve of Z_C vs. T_C . Numerical results based on Equation (38) are shown later in the paper.

3. Results and Discussion

3.1. Efficacy Spatial Profiles

As shown by Equation (31), the S function also defines the monomer conversion efficacy given by $C_{EFF} = 1 - \exp(-S)$, and S has a transient state function $E(z,t)$, governed by the dynamic profiles of the light intensity $I(z,t)$ and PI concentration, $C(z,t)$, given by Equations (28) and (29). Based on Equations (19) and (31), the spatial profiles of the conversion efficacies of the monomer [B] (or ene) are shown in Figure 3; for a fixed light intensity, efficacy is an increasing function of exposure time (t), but a decreasing function of the depth (z). Similarly, Figure 4 shows that the efficacy is an increasing function of light intensity (for a fixed exposure time). However, for very large exposure times, with an S function approaching its steady state, with $E(z,t) = 1$ in Equation (32), the efficacy becomes an increasing function of z , as reported by our previous studies [15,16] which also discussed the scaling laws of the S function in greater details.

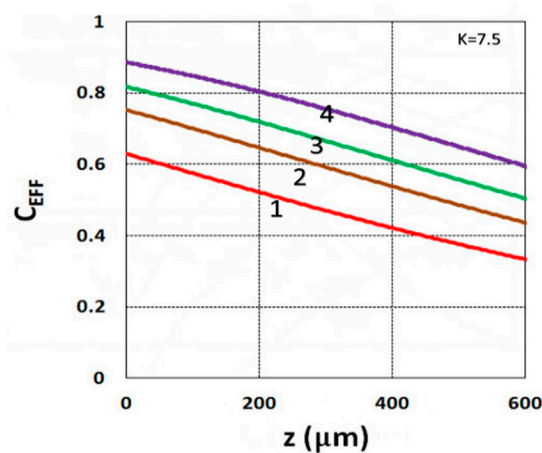


Figure 4. Conversion efficacy vs. depth (z) for $I_0 = (1, 2, 3, 5) \text{ mW/cm}^2$, given by curves 1, 2, 3, and 4, respectively, for $t = 20 \text{ s}$.

3.2. Dynamic Profiles of the Light Intensity

Figure 5 shows the dynamic profiles of the PI-normalized concentration and the increase of light intensity obtained by the numerical solution of Equation (1). Depending on the coupling parameters b and A , as shown by Equation (30), the depletion of $C(z,t)$ causes the increasing $I(z,t)$, defined by an increasing percentage $dI = [I(z,t) - I_0]/I_0$, which is also a decreasing function of the depth (z), per the Beer–Lambert law. Figure 6 shows an increase of 6% to 10% light intensity (at $z = 100 \mu\text{m}$) for $b = 0.05$ to 0.2 , $a' = 200$ (1%/mM), $b' = 100$ (1/cm/%), $Q = 50$ (1/cm), and $I_0 = 5 \text{ mW/cm}^2$. Figure 6 shows that larger b values had a faster PI depletion and hence a larger light intensity increase. For thick polymers ($>100 \mu\text{m}$), the conversion efficacies of the thiol (C_T) and ene (C_V) functional groups are also depth (z)-dependent, as well as time-dependent. The example shown in Figure 5 demonstrates that the assumption of constant light intensity and PI concentration is valid only for optically thin ($<100 \mu\text{m}$) polymers under a small dose ($<1.0 \text{ mJ/cm}^2$), i.e., under the condition of Equation (9c) with $B' = 2.3(a' - b') b C_0 I_0 t z < 0.1$. For optically thick polymers under a larger dose, with $b I_0 t z = 0.1$ to 0.2 , the thin-polymer model assumption will cause an error of 5% to 20%, depending on the depth of light propagation or polymer thickness, and its absorption coefficient. The influence of B' on the crosslink depth and efficacy is shown later in the paper. Note also that, as shown by Equation (3), the photoinitiation rate function (R_P) is proportional to the product of $I(z,t)$ and $C(z,t)$, which are two competing parameters, as shown by Figure 5. Therefore, there are optimal values of $I(z,t)$ and $C(z,t)$, as shown earlier in Figures 3 and 4.

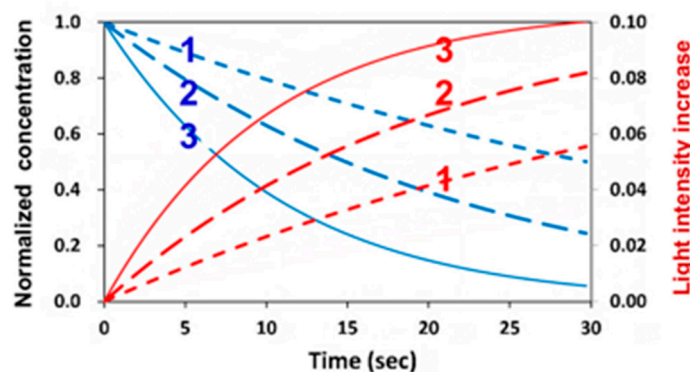


Figure 5. Dynamic profiles of normalized photoinitiator (PI) concentration (blue curves) and light intensity increases dI (red curves) for $b = (0.05, 0.1, 0.2)$, for curves 1,2,3.

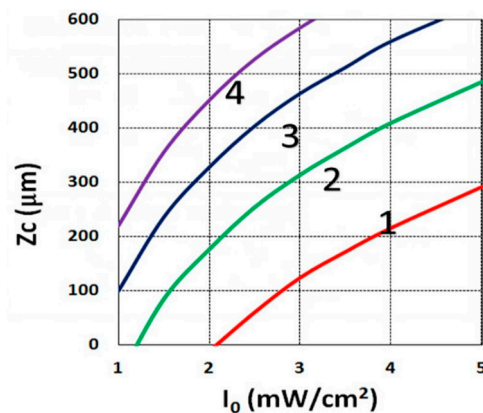


Figure 6. Crosslink depth (Z_C) vs. light intensity (I_0) for $t = (15, 20, 25, 30) \text{ s}$, given by curves 1, 2, 3, and 4, respectively, for $C_0 = 0.1\%$, based on Equation (14), for $B' = 0$.

3.3. Crosslink Depth Profiles

Using the analytical formula Equation (38), we were able to investigate the roles of PI, oxygen concentration, light intensity, and exposure time in crosslink depth. Figure 6 shows that crosslink depth (Z_C) (for the case of $B' = 0$) is an increasing function of light intensity and exposure time. Figure 7 shows the influence of dynamic light intensity due to PI depletion given by B' in Equation (30): that the assumption of $B' = 0$ suffers an error of 10% to 20% (underestimated) of Z_C for depths of 300 to 500 μm . Therefore, the assumption is valid only for optically thin polymer thinner than 200 μm for the case of absorption constant $a' = 130$, and thinner than 100 μm for a stronger absorption of 260 ($1/\text{cm}/\%$), or when $C_0 = 0.2\%$, as shown by Equation (9), $B' = 2.3(a' - b') C_0 I_0 z$. The influence of B' on the efficacy profiles is shown in Figure 8, namely that neglecting the B' factor also results in an underestimation of the efficacy.

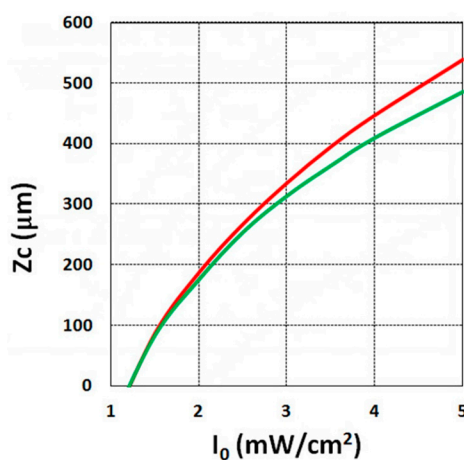


Figure 7. Crosslink depth (Z_C) vs. light intensity (I_0), for $B' = 0$ (green curve), and $B' = 0.06I_0z > 0$ (red curve) for $C_0 = 0.1\%$, $t = 20$ s.

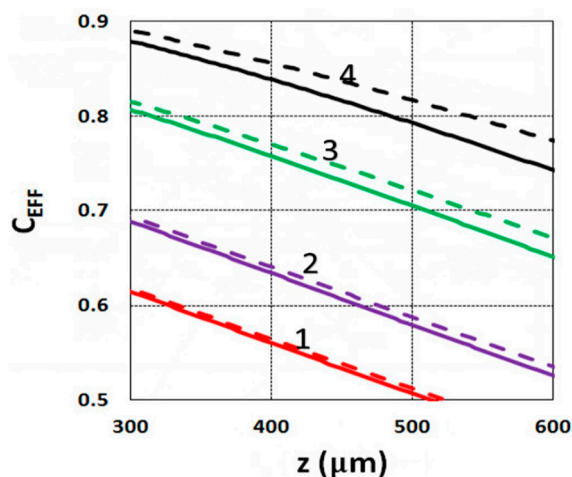


Figure 8. Efficacy vs. depth (z) based on Equation (14) for $I_0 = (1, 2, 3, 5)$ mW/cm^2 , given by curves 1, 2, 3, and 4, respectively, at $t = 20$ s, $C_0 = 0.1\%$; for $B' = 0$ (solid curves), and $B' = 0.06I_0z$ (dashed curves).

3.4. Numerical Results of Conversion

This section shows the numerical results of the conversion efficacy of thiol and various ene functional groups by solving Equation (1) to (10). These numerical data were analyzed by our analytic formulas and compared with the experimental data of Cramers et al. [18]. We also demonstrated that our modeling for a thiol–acrylate system including homopolymerization effects, and for a thiol–norbornene

system including viscosity effects, fit much better with the measured data than the model of Cramers et al. [18] for the high efficacy region.

Figure 9 shows the conversion efficacy of ene, [B], for a fixed $z = 100 \mu\text{m}$, with a rate ratio $R_K = k_p/k_{CT} = 0.2$, for various light intensity of $I_0 = (1, 5, 25) \text{ mW/cm}^2$, which demonstrates that, for a fixed light dose, higher light intensity has a higher transient efficacy, but a lower steady-state conversion. These numerically obtained features were also predicted by Equation (10), and may be compared with Figure 5.

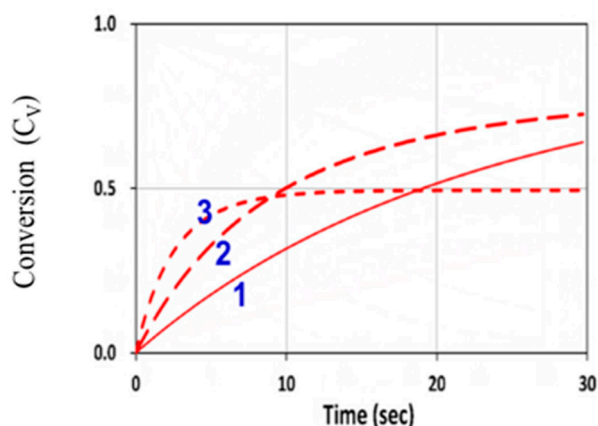


Figure 9. Conversion efficacy of ene (C_V) vs. time at various light intensity of $I_0 = (1, 5, 25) \text{ mW/cm}^2$, given by curves 1, 2, and 3, respectively, for $b = 0.05$, $k_p = 0.1 \times 10^5$, $k_{CT} = 2 \times 10^5$ (with a rate ratio $R_K = k_p/k_{CT} = 0.2$), $k_T = 1 \times 10^6 \text{ (L/mol.s)}$, and $[A]_0 = [B]_0 = 5.0 \text{ mol/L}$, neglecting the viscosity and homopolymerization effects (or $k_{CV} = 0$ and $F = 1$).

We next explored the roles of the rate ratio $R_K = k_p/k_{CT}$ for various concentration ratios $R_C = [A]_0/[B]_0$. For $k_{CV} = 0$ and $F = 1$, the G function of Equation (16) was the same for Equations (13) and (14), which are symmetric equations. Therefore, [A] and [B] had identical solutions, except that their dependence on R_C is reversed, i.e., [B] was governed by $[B]_0/[A]_0$ and [A] by $[A]_0/[B]_0$. These opposite dependences on the concentration ratio R_C lead to the reversed curves of 1 and 3 in Figure 10 for [B] and [A]. These features seem unexpected numerically, but they were clearly predicted by our analytical formulas, Equations (24) and (26), for the case that $k_{CV} = 0$ and $F = 1$, or when the homopolymerization and viscosity effects were neglected.

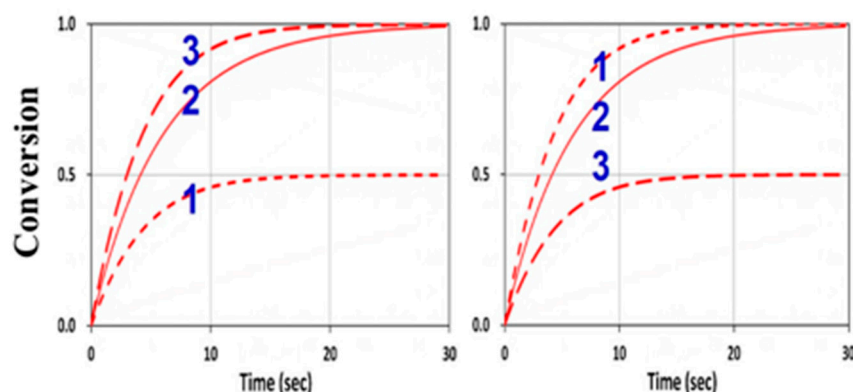


Figure 10. Conversion efficacy of ene (left) and thiol (right) for $R_K = 1.0$ and various concentration ratios $R_C = [A]_0/[B]_0 = (0.5, 1.0, 2.0)$, given by curves 1, 2, and 3, respectively, neglecting the viscosity and homopolymerization effects ($k_{CV} = 0$ and $F = 1$).

3.5. Analysis of Measured Data

Figure 11 shows the conversion in a thiol–vinyl system, using the same parameters used in Figure 4 from Cramers et al. [18], with $R_K = k_P/k_{CT} = 0.2$ and $k_{CV} = 0$, for various $R_C = (0.5, 1.0, 2.0)$. Our calculated curves fit very well with the measured data of Cramers et al. (with fit $b = 0.01$).

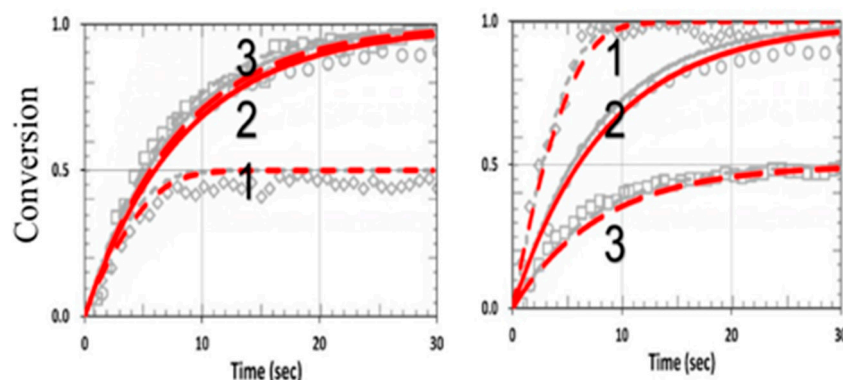


Figure 11. Calculated conversion efficacy of vinyl (left) and thiol (right), for $k_P = k_{CP} = 1.0 \times 10^5$, (or $R_K = 1.0$), $k_T = 1 \times 10^6$ (L/mol.s), and various concentration ratios $R_C = [A]_0/[B]_0 = (0.5, 1.0, 2.0)$, given by curves 1, 2, and 3, respectively; the background gray circles are the measured data of Cramer et al. [18].

Figure 12 shows the effects of homopolymerization (with $k_{CV} = 0.25 \times 10^5$) in a thiol–acrylate system, using the same parameters used in Figure 13 from Cramers et al. [18] with $k_P/k_{CT} = 13$, but also including the dynamic light intensity and PI depletion. The modeling data of Cramers et al. were consistent with ours for specific values of b and z . However, for different PI concentration profiles (or different b), or polymer thicknesses (z), the conversion efficacies of thiol and ene were changed accordingly. As predicted by Equations (24) and (25), the conversion efficacy of thiol [A] did not affected by H_M or k_{CV} . In contrast, as predicted by Equation (27), the efficacy of acrylate [B] increased when k_{CV} increased. This feature was also shown by our numerical data presented in Figure 11, in which our model fit very well the measured data of Cramer et al. [18], except for the transient region in which we neglected the induction time (or lag period) due to the initial interaction of the functional groups and the impurities or oxygen. Therefore, a further improved model including induction time would be needed for strong induction systems as discussed by Claudino et al. [22].

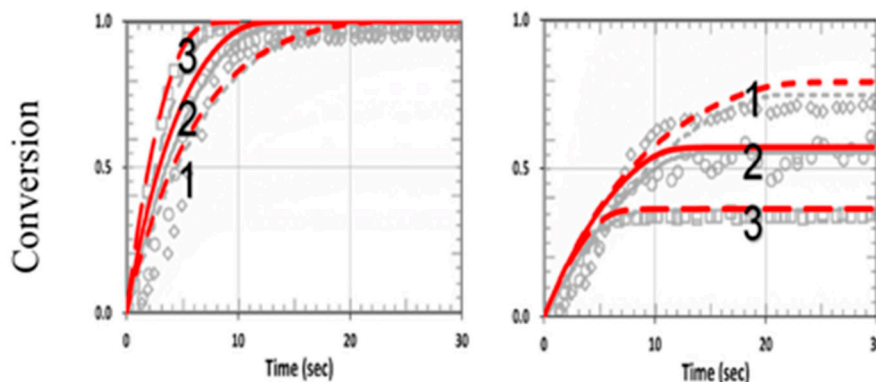


Figure 12. Calculated conversion efficacy of acrylate (left) and thiol (right), for $k_P = 2.2 \times 10^5$, $k_{CP} = 0.17 \times 10^5$ (or $R_K = 13$), and various concentration ratios $R_C = [A]_0/[B]_0 = (0.5, 1.0, 2.0)$, including homopolymerization effects (with $k_{CV} = 0.25 \times 10^5$). The background gray circles are the measured data of Cramer et al. [18].

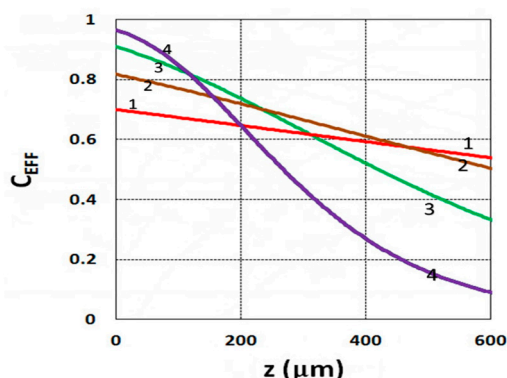


Figure 13. Conversion efficacy vs. depth (z) for $C_0 = (0.05, 0.1, 0.2, 0.4)$ %, given by curves 1, 2, 3, and 4, respectively, for $I_0 = 3 \text{ mW/cm}^2$ at $t = 20 \text{ s}$.

Figure 14 shows the viscosity effect on the conversion efficacy using the same parameters shown in Figure 2 from Cramers et al. [18], with $k_P = k_{CP} = 1.0 \times 10^5$ (or $R_K = 1.0$) for a thiol–norbornene system. Note that the model-predicted conversions of Cramers et al. (shown by black curves) were higher than their measured data, due to their assumption of a constant reaction rate (k_P). In our revised model, we included a reduction factor ($F < 1$) in Equation (22) for the viscosity effect, which reduces the available free volume specifically for the high efficacy region. We propose that $F = 1 - [1 - \exp(-S')]$, with S' proportional to the efficacy and given by a fit function $S' = 2[1 - \exp(-mb'I_0t)]/(mb'I_0)^{0.5}$, with $m = 0.5$ and $b' = 0.03$ fit to the measured data, as in Figure 2 of Cramers et al. [18]. The reduction factor is proportional to the available free volume, or a decreasing function of the conversion efficacy, which is proportional to S' . As shown in Figure 14, a much better fit to the measured curves was found in our revised model (shown by red curves). Note that without the viscosity effect (or $k_{CV} = 0$, $F = 1$), Figure 14 reduces to Figure 11, in which the symmetrical feature of C_V and C_T becomes asymmetrical, resulting from the viscosity effect, which mainly affects the propagation parameter of norbornene (k_P). This reduction factor (F) affects both C_V and C_T specifically for the case of $k_P = k_{CT}$ (or $R_K = 1.0$). Note that the modeling curves in Figure 2 of Cramers et al. [18] are the same as in our Figure 11 (with $k_{CV} = 0$, $F = 1$).

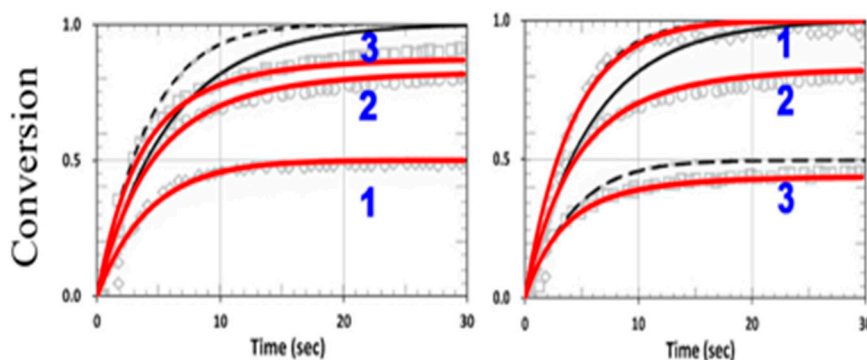


Figure 14. Calculated conversion efficacy of norbornene (left) and thiol (right), including the viscosity effects (with a reduction factor, $F < 1$), for various concentration ratios $R_C = [A]_0/[B]_0 = (0.5, 1.0, 2.0)$, for curves 1,2,3; with $k_P = k_{CT} = 1.0 \times 10^5$ ($R_K = 1.0$). The calculated curves without (in black dash) and with (in red) the viscosity effects are also shown.

3.6. General Features of Conversion Efficacy

Our numerical results for the conversion efficacies C_T (for thiol [A]) and C_V (for ene [B]) showed that the roles of the reaction rate ratio, $R_K = k_P/k_{CT}$, and the concentration ratio, $R_C = [A]_0/[B]_0$, were

consistent with our predicted results based on analytical formulas which provided more general features for the roles of R_K and R_C , summarized as follows:

Without viscosity (with $F = 1$) or homopolymerization (or $k_{CV} = 0$) effects, $[A]$ and $[B]$ have an equal overall polymerization rate (R_P); C_V (C_T) is an increasing (decreasing) function of the ratio R_C . For $R_K = 1$ (or $k_p = k_{CT}$), C_V and C_T have the same temporal profiles, but have a reversed dependence on R_C , as shown by Figure 10.

For $R_K \ll 1$, $[B]$ and C_V are almost independent from R_C , with a second-order correction proportional to R_C having asymmetrical dependence on R_C , given by $(1 - d)$, with $d = R_K/R_C$, as shown by Figure 11.

For $R_K \gg 1$, $[A]$ and C_T are almost independent from R_C , but the second-order correction is inversely proportional to R_C , an opposite trend to that of C_V . As predicted by Equation (25), the first-order solutions (with neglected $d = 0$) of C_T and C_V were independent from R_C .

For $R_K \ll 1$ and with the homopolymerization effect considered (with $k_{CV} > 0$, $F' > 0$), a revised S function of Equation (21) and Equation (27) predicts that C_V and C_T would have the same profiles and both be decreasing functions of k_{CV} . In comparison, for the case of $R_K \gg 1$, k_{CV} does not affect $[A]$, as shown by Equation (26), which predicts that C_V is an increasing function of k_{CV} , but C_T is a slightly decreasing function of k_{CV} , due to its second-order correction.

With the presence of viscosity effect, or when $F < 1$, in Equation (22), the free-volume is reduced when crosslink efficacy increases. The reduction factor (F) only affects the propagation rate constant Fk_p in Equations (20) and (22), but not in Equation (25). Therefore, the viscosity effect does not affect the efficacy for the case of $R_K \gg 1$, and affects the efficacy for other ratios of k_p and k_{CT} , where the viscosity effect reduces the efficacy of $[B]$, as predicted by Equation (22).

As predicted by the analytical formula of Equation (31) and the numerical data of Figure 9, for a fixed light dose, higher light intensity has a higher transient efficacy, but a lower steady-state conversion. This unique and unusual feature of the light intensity dependence is the result of a bimolecular termination. In contrast, in type II unimolecular termination, the conversion is mainly governed by the light dose, rather than its intensity.

For optically thick polymers, the influence of dynamic light intensity due to PI depletion is given by B' in Equation (30), which predicts that the assumption of $B' = 0$ (as in most previous models) suffers an error of 5% to 20% (underestimated) for a crosslink depth (Z_C) ranging 300 to 500 μm , and also underestimates the efficacy, as shown by Figures 7 and 8.

Scaling laws for the functional group concentration of thiol, $[A]$, and ene, $[B]$ are given by $[A]^m[B]^n$. For $R_K \gg 1$, the polymerization rates are first order in the ene concentration (or $n = 1.0$) and nearly independent of the thiol concentration (or $m = 0$); in contrast, $m = 1.0$ and $n = 0$ for $R_K \ll 1$. For R_K values near unity, polymerization rates are approximately 0.5 order in both thiol and ene functional group concentrations ($m = n = 0.5$). However, a scaling law of $m = 0.4$ and $n = 0.6$ was found in an acrylate system (with $R_K = 13$), due to contributions from homopolymerization.

Based on the above-described general features for thiol–ene polymer systems, it is possible to tailor the two ratios, R_K and R_C , and choose the appropriate ene functional group to minimize side effects such as viscosity and homopolymerization for maximal monomer conversion or tunable degree of crosslinking. The binary thiol–vinyl system used in this study may be expended for multiple-component systems, such as the ternary thiol–ene–ene and thiol–ene–acrylate systems reported by Reddy et al. [20]. Furthermore, the model and formulas developed for the free-radical-mediated thiol–ene system may be extended (to be published elsewhere) for anionic chain process such as base-catalyzed, thiol–Michael addition reactions [26]. Further information on the monomer properties discussed in this article and the factors influencing photopolymerization kinetics and optimal materials with low molecular weight, low viscosity, and in situ polymerization mechanisms have been reported in earlier publications [28–30].

4. Conclusions

We demonstrated that our model for a thiol–acrylate system including homopolymerization effects, and for a thiol–norbornene system including viscosity effects, fit much better with the measured data than the previous model. Furthermore, we found that the dynamic light intensity due to photoinitiator depletion cannot be neglected in optically thick polymers. The efficacies of the thiols and enes depend on both R_K and R_C , which may be tailored together with the choice of ene functional group to minimize side effects such as viscosity and homopolymerization for maximal conversion efficacy.

Author Contributions: Conceptualization, J.-T.L.; Data curation, K.-T.C. and D.-C.C.; Formal analysis, J.-T.L. and D.-C.C.; Funding acquisition, H.-W.L. and D.-C.C.; Methodology, J.-T.L.; Software, K.-T.C. and D.-C.C.; Supervision, J.-T.L. and H.-W.L.; Validation, J.-T.L. and K.-T.C.; Visualization, J.-T.L. and H.-W.L.; Writing—original draft, J.-T.L.; Writing—review & editing, J.-T.L.

Funding: This research received no external funding, and the APC was funded by China Medical University, Taiwan, ROC.

Conflicts of Interest: The authors declare no conflict of interest.

References

1. Fouassier, J.P. *Photoinitiation, Photo-Polymerization, and Photocuring: Fundamentals and Applications*; Hanser Gardner Publications: Munich, Germany, 1995.
2. Odian, G. *Principles of Polymerization*, 4th ed.; John Wiley & Sons, Inc.: New York, NY, USA, 2006.
3. Chen, F.M.; Shi, S. *Principles of Tissue Engineering*, 4th ed.; Elsevier: New York, NY, USA, 2014.
4. Hafezi, F.; Randleman, J.B. (Eds.) *Corneal Collagen Cross-Linking*, 2nd ed.; SLACK: Thorofare, NJ, USA, 2016.
5. Wohlers, T.; Caffrey, T. *Wohlers Report 2016: 3D Printing and Additive Manufacturing State of the Industry*; Annual Worldwide Progress Report; Wohlers Associates, Inc.: Fort Collins, CO, USA, 2016.
6. Chen, F.H.; Pathreker, S.B.; Hosein, I.D. Synthesis of Micropillar Arrays via Photopolymerization: An In Situ Study of Light-Induced Formation, Growth Kinetics, and the Influence of Oxygen Inhibition. *Macromolecules* **2017**, *50*, 5767–5778. [[CrossRef](#)]
7. Cabral, J.T.; Hudson, S.D.; Harrison, C.; Douglas, J.F. Frontal Photopolymerization for Microfluidic Applications. *Langmuir* **2004**, *20*, 10020–10029. [[CrossRef](#)] [[PubMed](#)]
8. O'Brien, A.K.; Bowman, C.N. Modeling the effect of oxygen on photopolymerization kinetics. *Macromol. Theory Simul.* **2006**, *15*, 176–182. [[CrossRef](#)]
9. Dendukuri, D.; Panda, P.; Haghgoie RKim, J.M.; Hatton, T.A.; Doyle, P.S. Modeling of Oxygen-Inhibited Free Radical Photopolymerization in a PDMS Microfluidic Device. *Macromolecules* **2008**, *41*, 8547–8556. [[CrossRef](#)]
10. Stockmayer, W.H. Theory of molecular size distribution and gel formation in branched polymers II. general cross linking. *J. Chem. Phys.* **2004**, *12*, 125. [[CrossRef](#)]
11. Alvankarian, J.; Majlis, B.Y. Exploiting the Oxygen Inhibitory Effect on UV Curing in Microfabrication: A Modified Lithography Technique. *PLoS ONE* **2015**, *10*, e0119658. [[CrossRef](#)] [[PubMed](#)]
12. Wu, J.; Zhao, Z.; Hamel, C.M.; Mu, X.; Kuang, X.; Guo, Z.; Qi, H.J. Evolution of material properties during free radical photopolymerization. *J. Mechan. Phys. Solid.* **2018**, *112*, 25–49. [[CrossRef](#)]
13. Lin, J.T. Efficacy S-formula and kinetics of oxygen-mediated (type-II) and non-oxygen-mediated (type-I) corneal cross-linking. *Ophthalmol. Res.* **2018**, *8*, 1–11. [[CrossRef](#)]
14. Lin, J.T.; Wang, K.C. Analytic formulas and numerical simulations for the dynamics of thick and non-uniform polymerization by a UV light. *J. Polym. Res.* **2016**, *23*, 53. [[CrossRef](#)]
15. Lin, J.T.; Cheng, D.C. Modeling the efficacy profiles of UV-light activated corneal collagen crosslinking. *PLoS ONE* **2017**, *12*, e0175002. [[CrossRef](#)]
16. Lin, J.T.; Liu, H.W.; Chen, K.T.; Cheng, D.C. Modeling the optimal conditions for improved efficacy and crosslink depth of photo-initiated polymerization. *Polymers* **2019**, *11*, 217. [[CrossRef](#)] [[PubMed](#)]
17. Chen, K.T.; Lin, J.T.; Liu, H.W. Enhancing radical-mediated photopolymerization efficacy and crosslink depth: Kinetic modeling of a two-monomer system. *Res. Med. Eng. Sci.* **2019**, *8*, 853–860.
18. Cramer, N.B.; Reddy, S.K.; O'Brien, A.K.; Bowman, C.N. Thiol-ene photopolymerization mechanism and rate limiting step for various vinyl functional group chemistries. *Macromolecules* **2003**, *36*, 7964–7969. [[CrossRef](#)]

19. Cramer, N.B.; Bowman, C.N. *Thiol-X Click Chemistries in Polymer and Materials Science*; Lowe, A.B., Bowman, C.N., Eds.; RSC Publishing: Cambridge, UK, 2013; p. 318.
20. Reddy, S.K.; Cramer, N.B.; Bowman, C.N. Thiol-Vinyl Mechanisms. 2. Kinetic Modeling of Ternary Thiol-Vinyl Photopolymerizations. *Macromolecules* **2006**, *39*, 3681–3687. [[CrossRef](#)]
21. Okay, O.; Bowman, C.N. Kinetic modeling of thiol-ene reactions with both step and chain growth aspects. *Macromol. Theory Simul.* **2005**, *14*, 267–277. [[CrossRef](#)]
22. Claudino, M.; Jonsson, M.; Johansson, M. Thiol-ene coupling kinetics of D-limonene: a versatile 'non-click' free-radical reaction involving a natural terpene. *RSC Adv.* **2013**, *3*, 11021–11034. [[CrossRef](#)]
23. Li, Y.; Su, H.; Feng, X.; Wang, Z.; Guo, K.; Wesdemiotis, C.; Fu, Q.; Cheng, S.Z.D.; Zhang, W.-B. Thiol-Michael "click" Chemistry: Another Efficient Tool for Head Functionalization of Giant Surfactants. *Polym. Chem.* **2014**, *5*, 6151–6162. [[CrossRef](#)]
24. Wang, C.; Zhang, X.; Podgoński, M.; Xi, W.; Shah, P.; Stansbury, J.; Bowman, C.N. Monodispersity/Narrow Polydispersity Cross-Linked Microparticles Prepared by Step-Growth Thiol-Michael Addition Dispersion Polymerizations. *Macromolecules* **2015**, *48*, 8461–8470. [[CrossRef](#)]
25. Zhang, X.; Xi, W.; Wang, C.; Podgoński, M.; Bowman, C.N. Visible-Light-Initiated Thiol-Michael Addition Polymerizations with Coumarin-Based Photobase Generators: Another Photoclick Reaction Strategy. *ACS Macro Lett.* **2016**, *5*, 229–233. [[CrossRef](#)]
26. Claudino, M.; Zhang, X.; Alim, M.D.; Podgoński, M.; Bowman, C.N. Mechanistic Kinetic Modeling of Thiol-Michael Addition Photopolymerizations via Photocaged "superbase" Generators: An Analytical Approach. *Macromolecules* **2016**, *49*, 8061–8074. [[CrossRef](#)] [[PubMed](#)]
27. Huang, S.; Sinha, J.; Podgoński, M.; Zhang, X.; Claudino, M.; Bowman, C.N. Mechanistic Modeling of the Thiol-Michael Addition Polymerization Kinetics: Structural Effects of the Thiol and Vinyl Monomers. *Macromolecules* **2018**, *51*, 5979–5988. [[CrossRef](#)]
28. Esposito Corcione, C.; Greco, A.; Maffezzoli, A. Photopolymerization kinetics of an epoxy based resin for setereolithography by calorimetric analysis. *J. Therm. Anal. Calorim.* **2003**, *72*, 687–693. [[CrossRef](#)]
29. Esposito Corcione, C.; Frigione, M. UV-cured siloxane-modified acrylic coatings containing birifrangent calcarenitic stone particles: Photo-calorimetric analysis and surface properties. *Prog. Org. Coat.* **2011**, *72*, 522–527. [[CrossRef](#)]
30. Esposito Corcione, C.; Frigione, M. Factors Influencing Photo-Curing Kinetics of Novel UV Cured Siloxane-Modified Acrylic Coatings: Oxygen Inhibition and Composition. *Thermochim. Acta* **2012**, *534*, 21–27. [[CrossRef](#)]



© 2019 by the authors. Licensee MDPI, Basel, Switzerland. This article is an open access article distributed under the terms and conditions of the Creative Commons Attribution (CC BY) license (<http://creativecommons.org/licenses/by/4.0/>).